

VELOCITY ESTIMATION FROM THE GPS TIME SERIES DATA



Shashi Kumar
Third Year Undergraduate
Indian Institute of Technology, Kharagpur

ABSTRACT

We have present two methods to derive secular plate velocity from GPS position time series that are affected by time-correlated noise. These methods are white noise method, power-law noise method and Markov Chain Monte Carlo (MCMC). Finally, we applied the method to the data collected from the IGS stations. We estimated the north and east component of the velocity and their uncertainties. Finally, we compared the results obtained from the three models.

Introduction

The Global Positioning System (GPS) is a space-based Global Navigation Satellite System (GNSS). Using signals transmitted by GPS satellites, the position of ground-based receivers can be calculated to high precision, making it possible to track the movement of points on the Earth's surface over time. GPS can provide three-component (latitude, longitude, and altitude) position information at a range of sampling rates and on a global scale. GPS has become indispensable for crustal deformation studies, leading to many important insights and some surprising discoveries.

GPS data provide important constraints on the underlying processes that lead to observed deformation. One of the major strength of GPS is its ability to track positions over time spans of seconds to decades. It enables measurement of position changes over continental scale baselines.

Earthquake occur in response to stresses in the Earth's crust, and these stresses are largely due to motion of the Earth's tectonic plates. Knowing the velocity at which the plates move gives us insight into the amount of deformation that must be accommodated on a plate boundary faults, and what type of earthquakes might be expected. The Earth's plates are generally thought to be rigid, at least in their interiors.

Nearly all GPS time series exhibit a seasonal cycle of displacement which can be modelled as 4-term Fourier series with periodicities of 1 year and 0.5 years. These cycles are caused by seasonal changes in water, snow, and ice loads or by seasonal changes in atmospheric pressure. But for this report we are only restricted to calculate the constant velocity trend. The displacement at the GPS sites can be estimated by the following relationship:

$$x(t) = a + b(t - t_0) + \epsilon$$

Where,

$x(t)$ = Displacement in mm.

t = Time in year

t_0 = Time at which observation starts (Set to 0)

a = Intercept term

b = Constant velocity in mm/year.

ϵ = Error term or noise in the data.

In the upcoming sections we are going to compute the parameters a and b with the help of different models and compare them.

Methodology

We can estimate the velocity parameter from the GPS time series through many methods. In this report we have provided three methods i.e. **White Noise Method**, **Power Law Noise Method** and **Markov Chain Monte Carlo (MCMC) Method**.

Geodetic time series consist out of a set of observations at various epochs. These observations, stored in a vector \mathbf{d} , are not perfect but contain noise, which can be described as a set of multivariate random variables.

Statistical analysis of geophysical data can be performed in two different ways: -

1. From a full knowledge of the parameter space, which is equivalent to having the distribution function.
2. On the other hand, from a data sample that accounts for the estimation of the distribution function.

3.1 White Noise Method

A white noise process is a random process of random variables that are uncorrelated, having zero mean, and a finite variance. They are independent from one another; formally, $x(t)$ is a white noise process if (E is the expectation function),

$$E(x(t)) = 0$$

$$E(x(t)^2) = S^2$$

$$E(x(t)x(\tau)) = 0, \quad t \neq \tau$$

The predicted observation can be written as:

$$\hat{d} = Am$$

Where,

\hat{d} = Predicted observation from the model

A = The design matrix.

m = Model Parameters

The noise in the observation can be written as:

$$\epsilon = d - \hat{d}, \quad (\epsilon \text{ is the noise term})$$

Using the Maximum Likelihood Estimation (MLE) on the noise, m can be written as:

$$m = (A^T C^{-1} A)^{-1} A^T C^{-1} d$$

The variance of the estimated parameter can be written as:

$$Var(m) = (A^T C^{-1} A)^{-1}$$

Where,

$$A = \begin{pmatrix} 1 & t_1 \\ \vdots & \vdots \\ 1 & t_n \end{pmatrix}, \quad m = \begin{pmatrix} a \\ b \end{pmatrix}, \quad d = \begin{pmatrix} d_1 \\ d_2 \\ \vdots \\ d_n \end{pmatrix}$$

$$C = \begin{pmatrix} 1 & \dots & 0 \\ 0 & \dots & 0 \\ \vdots & \ddots & \vdots \\ 0 & \dots & 1 \end{pmatrix}, \quad N \times N \text{ Identity Matrix}$$

3.2 Power Law Noise Method

Maximum Likelihood Estimation is a well-known technique in various branches of science. If there was no relation between each noise value, then these would be independent random variable and the covariance matrix, C would be zero except for values on its diagonal (Identity Matrix).

Practically, all geodetic time series, these are dependent random variable. In statistics, this is called temporal correlation and C can be written as:

$$C = \begin{pmatrix} \sigma_{11}^2 & \sigma_{12}^2 & \dots & \sigma_{1N}^2 \\ \vdots & \vdots & \ddots & \vdots \\ \sigma_{N1}^2 & \sigma_{N2}^2 & \dots & \sigma_{NN}^2 \end{pmatrix}$$

Where, σ_{12}^2 is the covariance between random variables w_1 and w_2 .

Most of the geophysical time series exhibit power-law noise behavior, that this type of modelling started to be applied to geodetic time series.

Power-law noise has the property that the power spectral density of the noise follows a power-law curve. The equation for power-law noise is:

$$P(f) = P_0 \left(\frac{f}{f_s}\right)^\kappa,$$

Where,

f is the frequency.

P_0 is a constant.

f_s is the sampling frequency.

κ is the called the spectral index.

Granger (1980), Granger and Joyeux (1980) and Hosking (1981) demonstrated that power-law noise can be achieved using fractional differencing of Gaussian noise:

$$(1 - B)^{-\kappa/2} v = w$$

Where,

B is the backward-shift operator ($B_{v_i} = v_{i-1}$)

v is the vector with independent and identically distributed (IID) Gaussian noise.

See Hosking and Granger (reference)

However, in geodesy the spectral index κ is used in the equations. Hosking's definition of the fractional differencing is:

$$\begin{aligned}
(1 - B)^{-\kappa/2} &= \sum_{i=0}^{\infty} \binom{-\frac{\kappa}{2}}{i} (-B)^i \\
&= 1 - \frac{\kappa}{2}B - \frac{1}{2}\frac{\kappa}{2}\left(1 - \frac{\kappa}{2}\right)B^2 + \dots \dots \dots \\
&= \sum_{i=0}^{\infty} h_i
\end{aligned}$$

The coefficients h_i can be viewed as a filter that is applied to the independent white noise. These coefficients can be conveniently computed using the following recurrence relation (Kasdin 1995):

$$\begin{aligned}
h_0 &= 1 \\
h_i &= \left(i - \frac{\kappa}{2} - 1\right) \frac{h_{i-1}}{i}, \quad \text{for } i > 0
\end{aligned}$$

The power-law covariance matrix can be calculated using the following relationship:

$$C(w_k, w_l) = \sum_{i=0}^k h_i h_{i+(l-k)}$$

$\kappa = 0$ produces an identity matrix, the associated white noise covariance matrix is represented by unit matrix I . The final covariance matrix is scaled by σ_{pl} , which is the noise amplitude. Since we don't know the value of κ and σ_{pl} , we can estimate them from the data using Maximum Likelihood Estimation(MLE).

3.3 Markov Chain Monte Carlo (MCMC) Method

A Markov chain is a series of random variables $X^{(0)}, X^{(1)}, X^{(2)}, \dots$ in which the influence of the values of $X^{(0)}, X^{(1)}, \dots, X^{(n)}$ on the distribution of $X^{(n+1)}$ is mediated by the value of $X^{(n)}$. In a more mathematical way,

$$P(X^{(n+1)} | X^{(0)}, X^{(1)}, \dots, X^{(N)}) = P(X^{(n+1)} | X^{(n)})$$

Where $P(X)$ denotes the probability of X , i.e. the probability that the value for the state variable x is X . A Markov chain can be specified by giving the prior and likelihood distribution.

For in depth information see chapter 1, 2 and 3 of **Geodetic Time Series Analysis in Earth Sciences** by Jean-Philippe Montillet and Machiel S. Bos. (<https://www.springer.com/gp/book/9783030217174>)

Data

All the GPS time series data used in this report has been downloaded from the UNAVCO. ([UNAVCO DAI](#)). We have collected data from 27 IGS Stations spread around the globe. (See Table 1 for the details)

GPS Sites

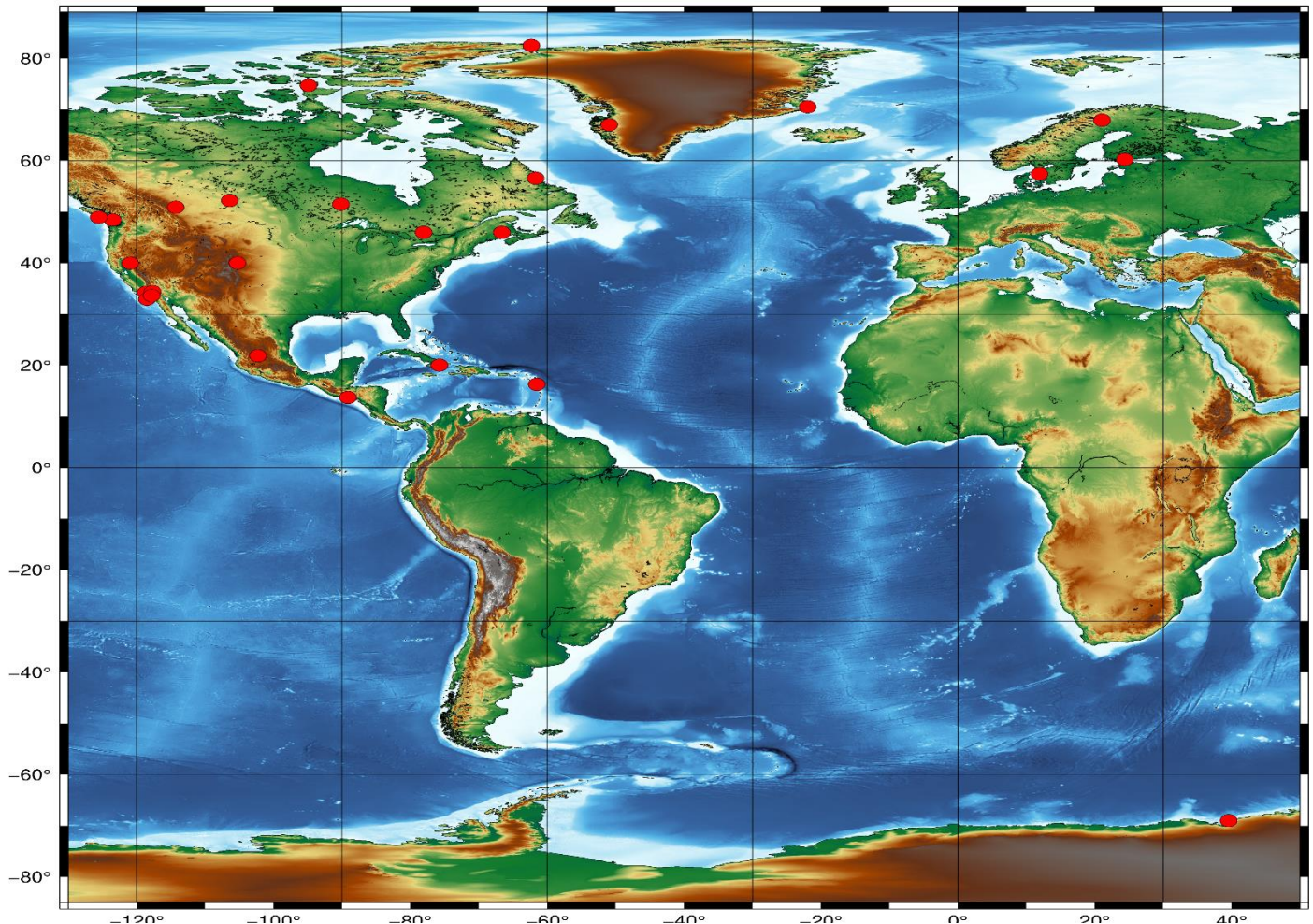


Figure 1 Location of GPS Sites (IGS).

Site Name	Latitude	Longitude	Start Date	End Date
ABMF	16.2623052386 N	-61.527536103 E	01-01-2015	24-05-2020
ALBH	48.3897811345 N	-123.4874707769 E	01-01-2015	15-09-2018
ALGO	45.9558003972 N	-78.0713685387 E	01-01-2015	15-09-2018
ALRT	82.4942938488 N	-62.3404653223 E	01-01-2015	15-09-2018
INEG	21.8561537703 N	-102.2842032442 E	01-01-2015	15-09-2018
JPLM	34.2048227188 N	-118.1732298658 E	14-01-2018	15-09-2018
KELY	66.9874185405 N	-50.9448388289 E	01-01-2015	30-05-2018
KIRO	67.8775766171 N	21.0602420393 E	01-01-2015	27-04-2020
METS	60.2174714851 N	24.3953235821 E	07-01-2018	15-09-2018
NAIN	56.5369757476 N	-61.6887171663 E	01-01-2015	15-09-2018
NIST	39.9950673112 N	-105.2626045199 E	14-01-2018	15-09-2018
ONSA	57.3952997130 N	11.9255182742 E	01-01-2015	27-04-2020
PICL	51.4798086828 N	-90.161975393 E	01-01-2015	24-05-2020
PRDS	50.8713512564 N	-114.2934980057 E	01-01-2015	24-05-2020
QUIN	39.9745538917 N	-120.9444290198 E	01-01-2015	24-05-2020
RESO	74.6908201876 N	-94.8936950804 E	01-01-2015	15-12-2017
ROCK	34.2356740341 N	-118.6764300401 E	01-01-2015	12-09-2018
SASK	52.1962546588 N	-106.3983555189 E	01-01-2015	15-09-2018
SCIP	32.9144276458 N	-118.4879389522 E	06-01-2015	15-09-2018
SCOR	70.4853345417 N	-21.9503379005 E	17-01-2015	15-09-2018
SCUB	20.0120635401 N	-75.7623166233 E	01-01-2015	11-09-2018
SSIA	13.6970852355 N	-89.1165949486 E	01-01-2015	03-05-2018
SYOG	-69.0069570924 N	39.5837429814 E	01-01-2015	29-09-2018
TABL	34.3818486437 N	-117.6782815256 E	01-01-2015	12-09-2018
TRAK	33.6179380068 N	-117.803437812 E	14-01-2018	15-09-2018
UCLU	48.9256375806 N	-125.5416410653 E	01-01-2015	15-09-2018
UNBJ	45.9502093181 N	-66.6417052075 E	01-01-2015	15-09-2018

Table 1: Start Date and End Date of the IGS sites along with their locations.

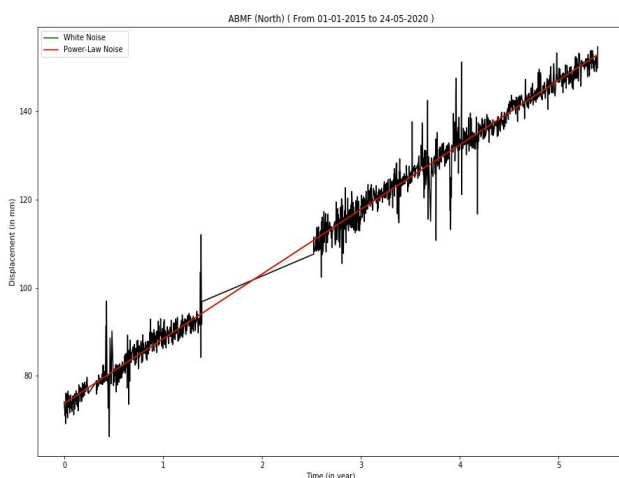
Analysis of GPS Time Series Data

We will estimate the model parameters using the methods listed in the methodology section of the North and East components of the displacement data.

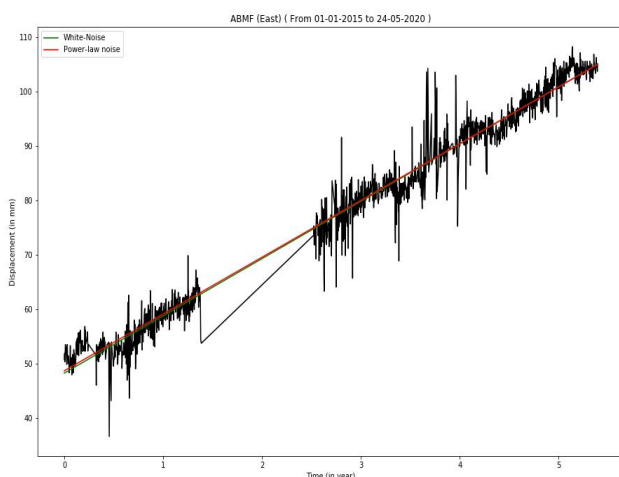
5.1 White Noise and Power-Law Noise

5.1.1 ABMF

- **Site Name:** ABMF
- **Location:** 16.2623052386 N , -61.527536103 E
- **Start Date:** 01-01-2015
- **End Date:** 24-05-2020



Northern Component

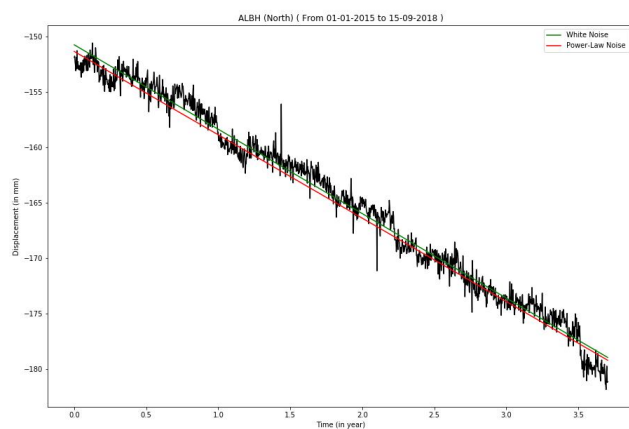


Eastern Component

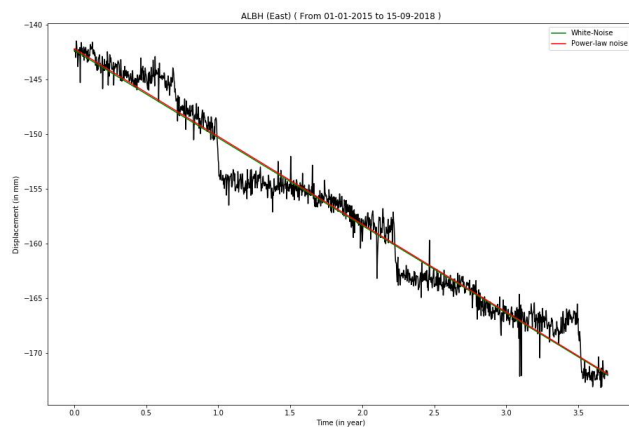
Figure 2

5.1.2 ALBH

- **Site Name:** ALBH
- **Location:** 48.3897811345 N, -123.4874707769 E
- **Start Date:** 01-01-2015
- **End Date:** 15-09-2018



Northern Component

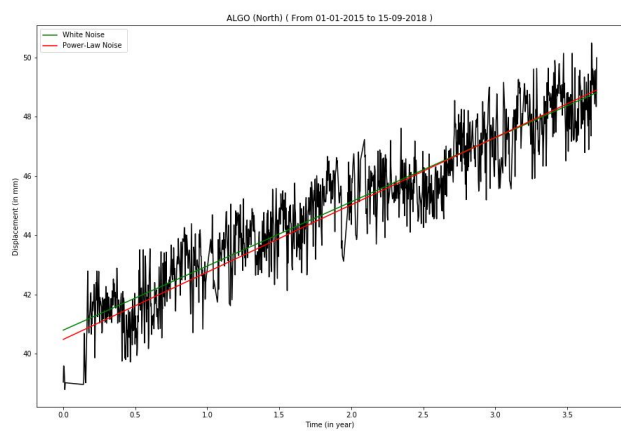


Eastern Component

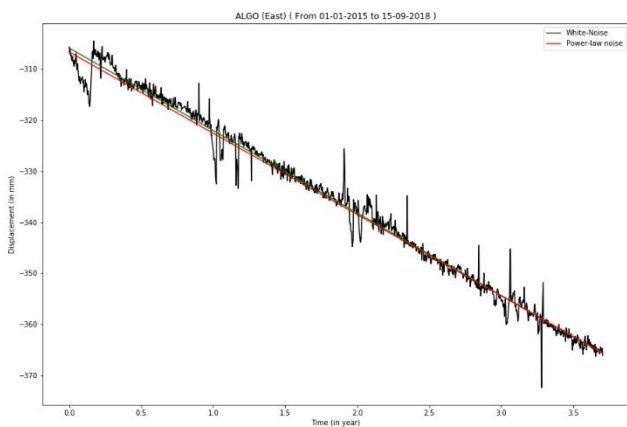
Figure 3

5.1.3 ALGO

- **Site Name:** ALGO
- **Location:** 45.9558003972 N, -78.0713685387 E
- **Start Date:** 01-01-2015
- **End Date:** 15-09-2018



Northern Component

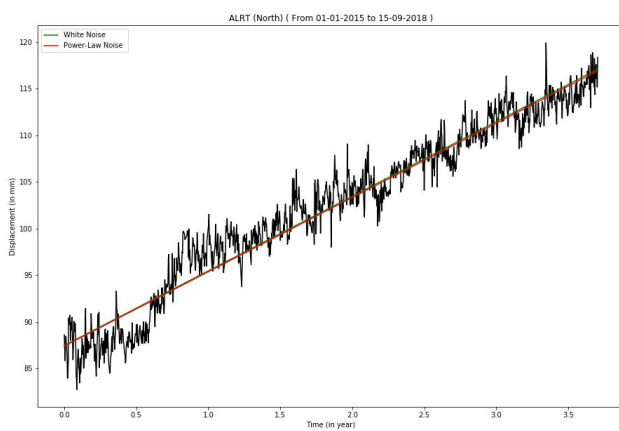


Eastern Component

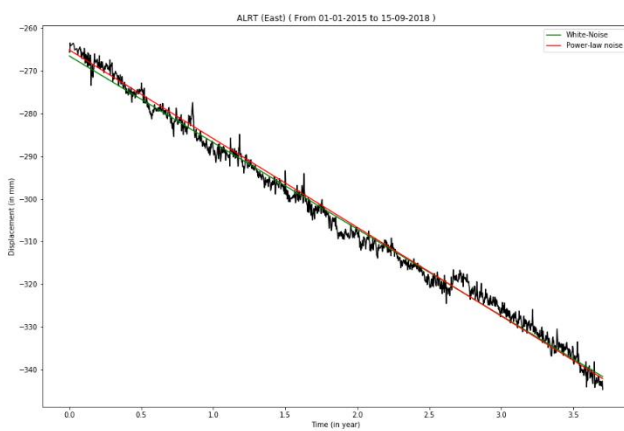
Figure 4

5.1.4 ALRT

- **Site Name:** ALRT
- **Location:** 82.4942938488 N, -62.3404653223 E
- **Start Date:** 01-01-2015
- **End Date:** 15-09-2018



Northern Component

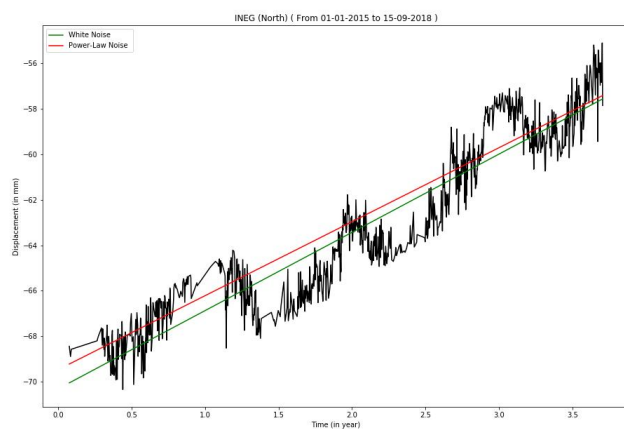


Eastern Component

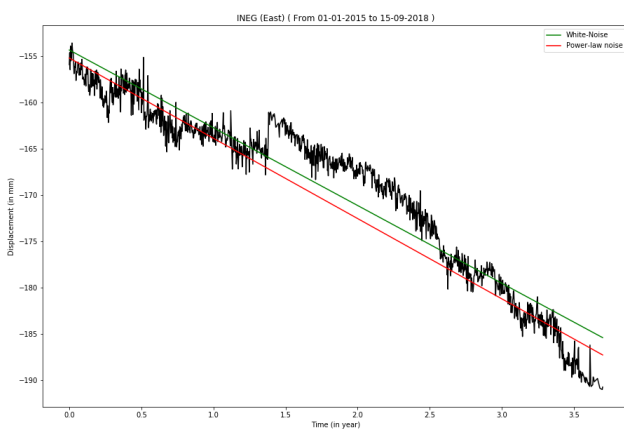
Figure 5

5.1.5 INEG

- **Site Name:** INEG
- **Location:** 21.8561537703 N, -102.2842032442 E
- **Start Date:** 01-01-2015
- **End Date:** 15-09-2018



Northern Component

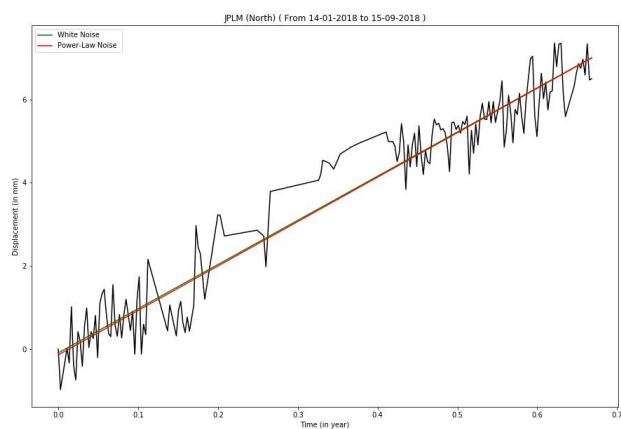


Eastern Component

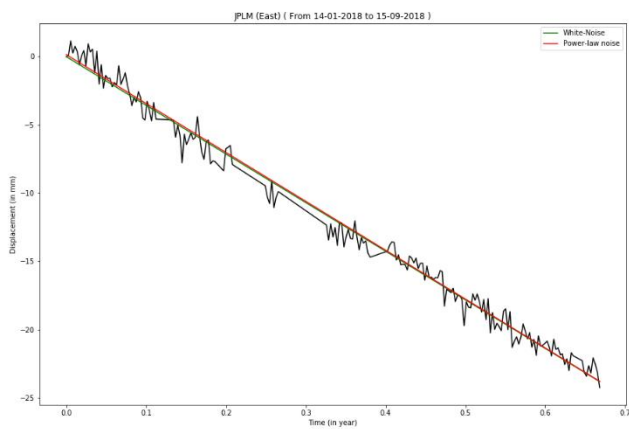
Figure 6

5.1.6 JPLM

- **Site Name:** JPLM
- **Location:** 34.2048227188 N, -118.1732298658 E
- **Start Date:** 14-01-2018
- **End Date:** 15-09-2018



Northern Component

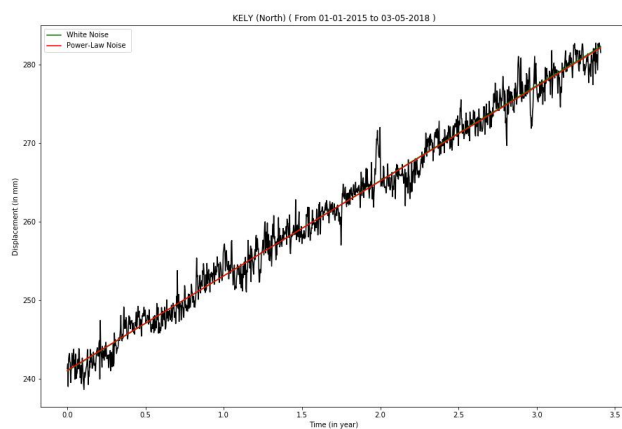


Eastern Component

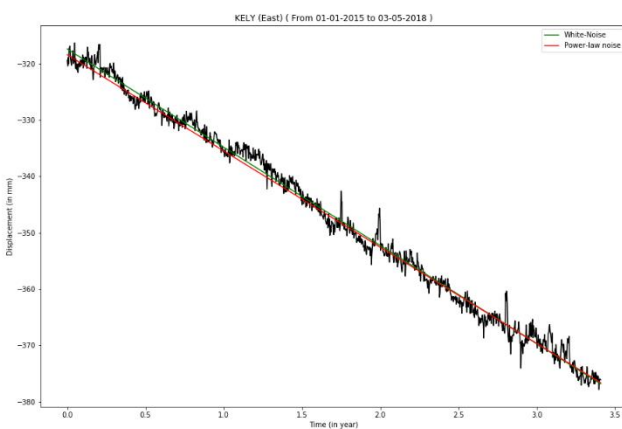
Figure 7

5.1.7 KELY

- **Site Name:** KELY
- **Location:** 66.9874185405 N, -50.9448388289 E
- **Start Date:** 01-01-2015
- **End Date:** 30-05-2018



Northern Component

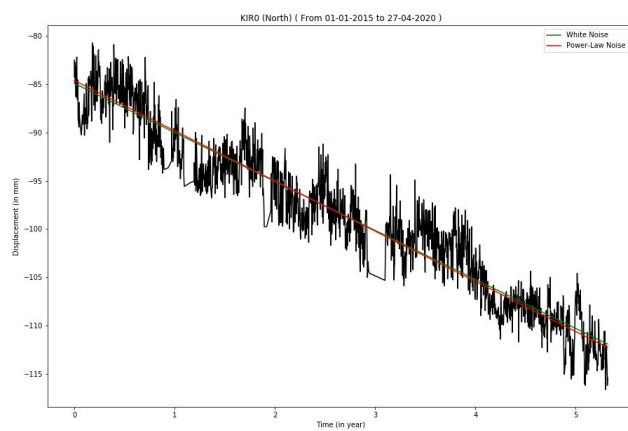


Eastern Component

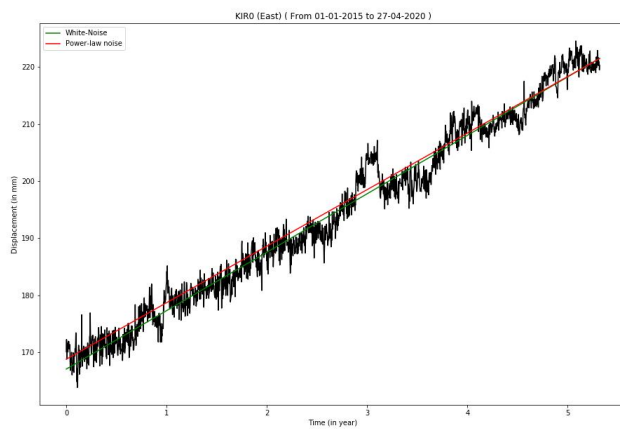
Figure 8

5.1.8 KIRO

- **Site Name:** KIRO
- **Location:** 67.8775766171 N, 21.0602420393 E
- **Start Date:** 01-01-2015
- **End Date:** 27-04-2020



Northern Component

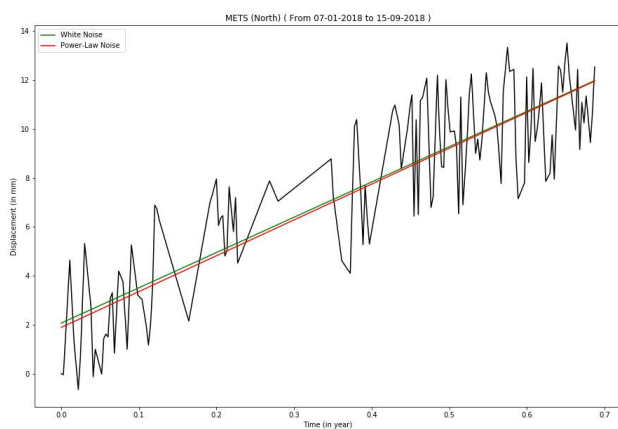


Eastern Component

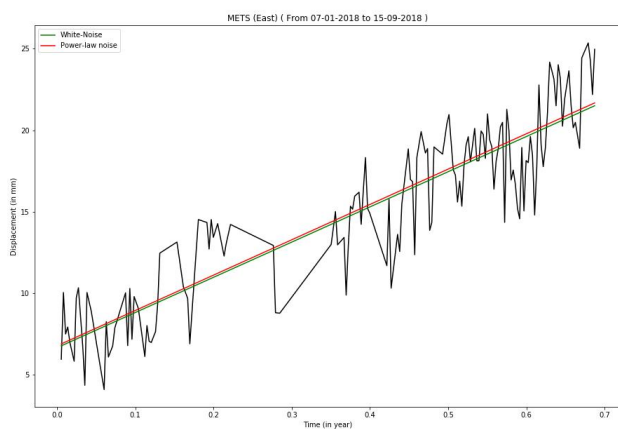
Figure 9

5.1.9 METS

- **Site Name:** METS
- **Location:** 60.2174714851 N, 24.3953235821 E
- **Start Date:** 07-01-2018
- **End Date:** 15-09-2018



Northern Component

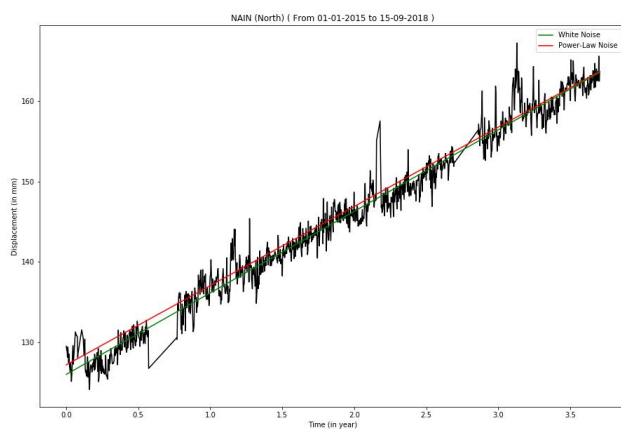


Eastern Component

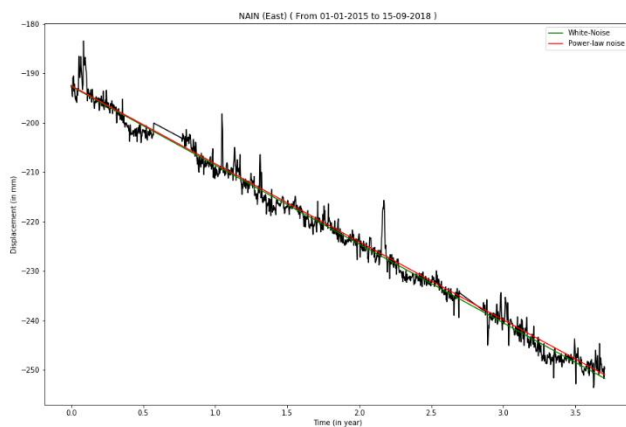
Figure 10

5.1.10 NAIN

- **Site Name:** NAIN
- **Location:** 56.5369757476 N, -61.6887171663 E
- **Start Date:** 01-01-2015
- **End Date:** 15-09-2018



Northern Component

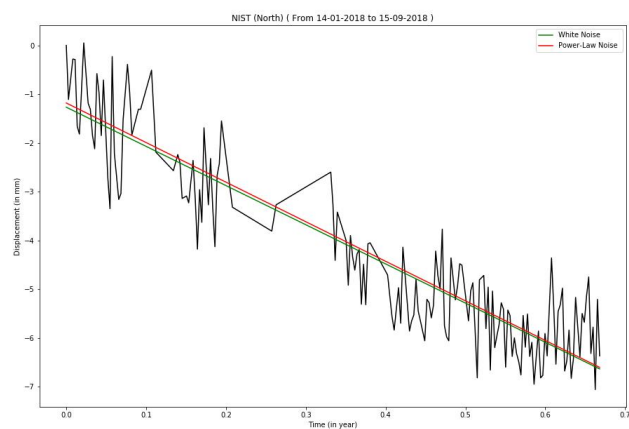


Eastern Component

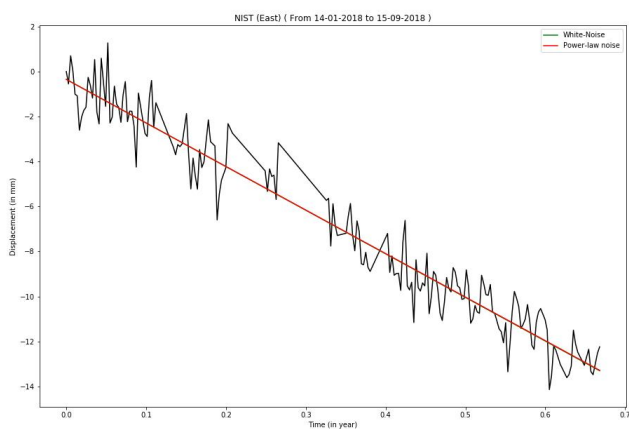
Figure 11

5.1.11 NIST

- **Site Name:** NIST
- **Location:** 39.9950673112 N, -105.2626045199 E
- **Start Date:** 15-01-2018
- **End Date:** 15-09-2018



Northern Component

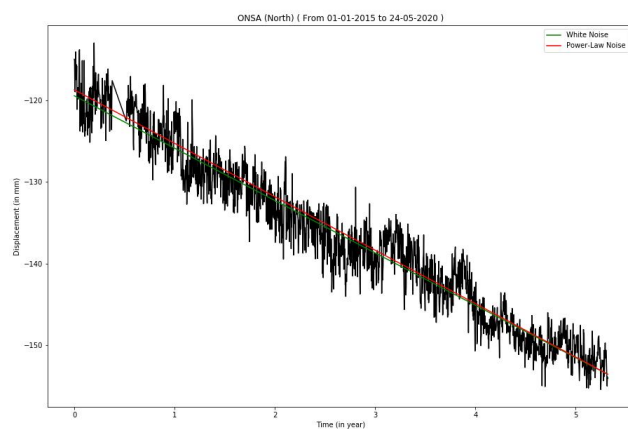


Eastern Component

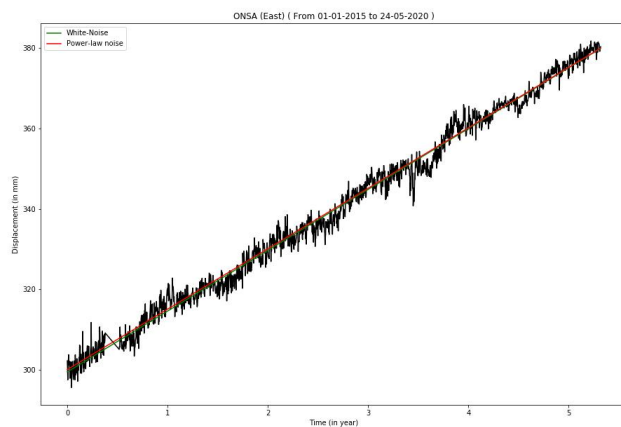
Figure 12

5.1.12 ONSA

- **Site Name:** ONSA
- **Location:** 57.3952997130 N, 11.9255182742 E
- **Start Date:** 01-01-2015
- **End Date:** 27-04-2020



Northern Component

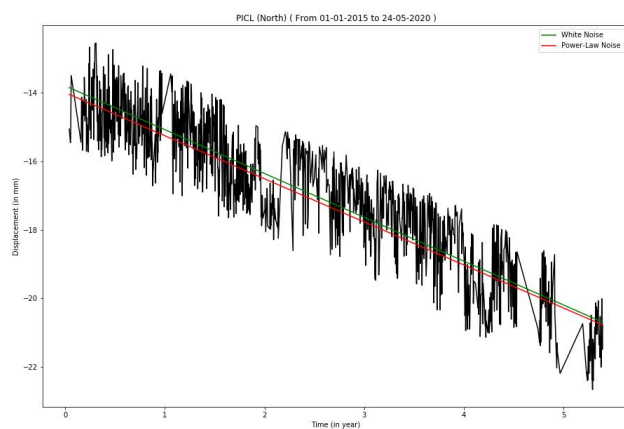


Eastern Component

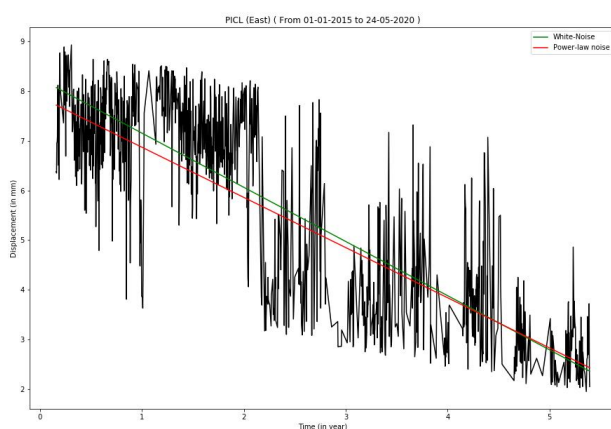
Figure 13

5.1.13 PICL

- **Site Name:** PICL
- **Location:** 51.4798086828 N, -90.161975393 E
- **Start Date:** 01-01-2015
- **End Date:** 24-05-2020



Northern Component

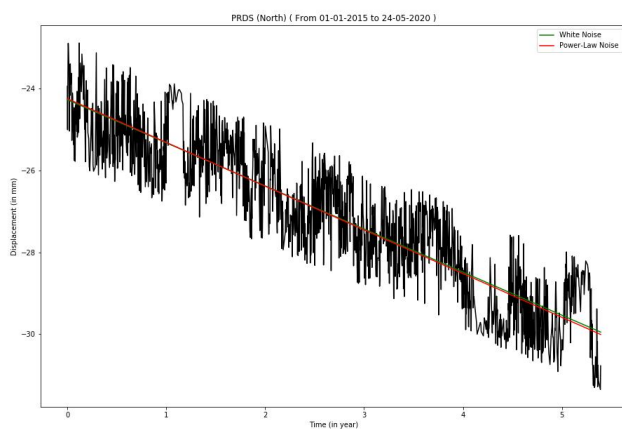


Eastern Component

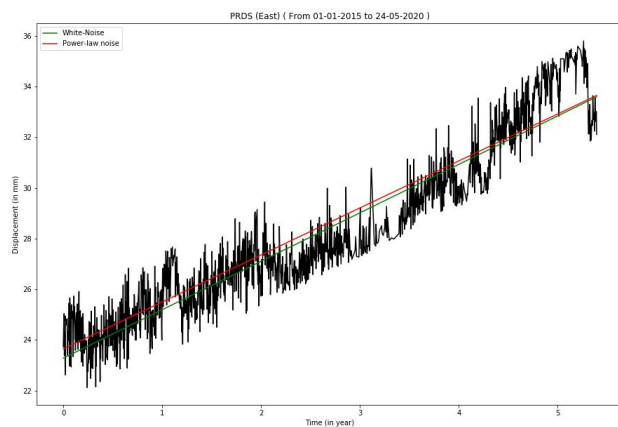
Figure 14

5.1.14 PRDS

- **Site Name:** PRDS
- **Location:** 50.8713512564 N, -114.2934980057 E
- **Start Date:** 01-01-2015
- **End Date:** 24-05-2020



Northern Component

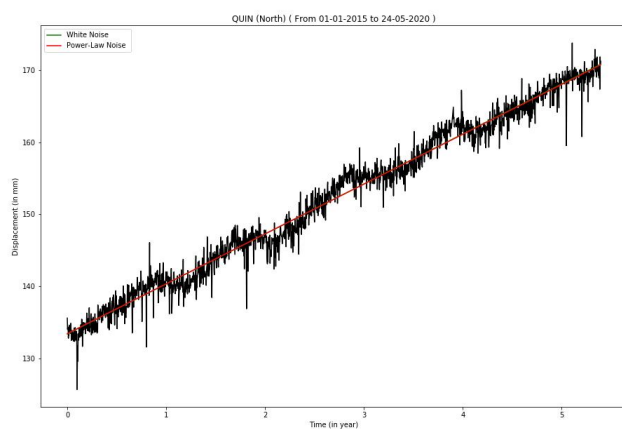


Eastern Component

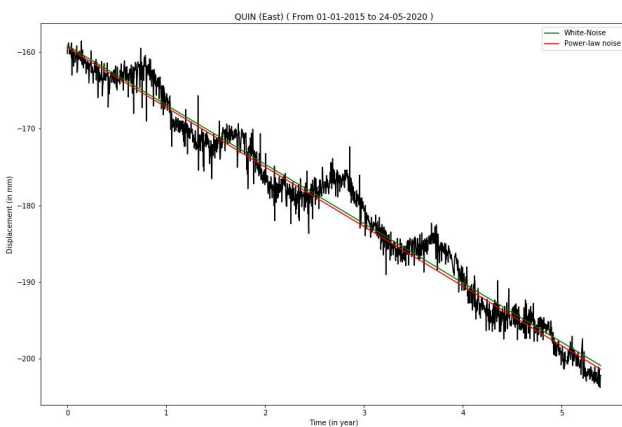
Figure 15

5.1.15 QUIN

- **Site Name:** QUIN
- **Location:** 39.9745538917 N, -120.9444290198 E
- **Start Date:** 01-01-2015
- **End Date:** 24-05-2020



Northern Component

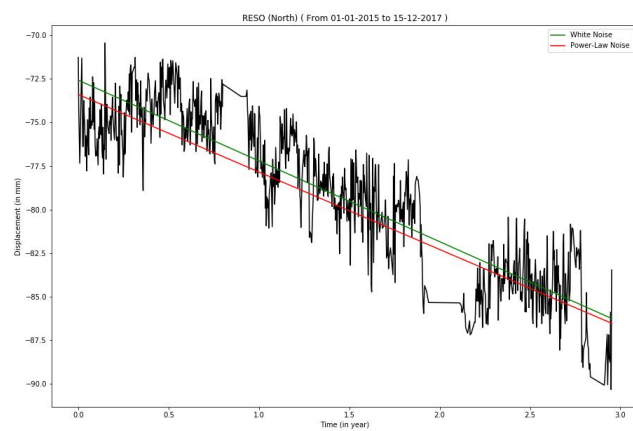


Eastern Component

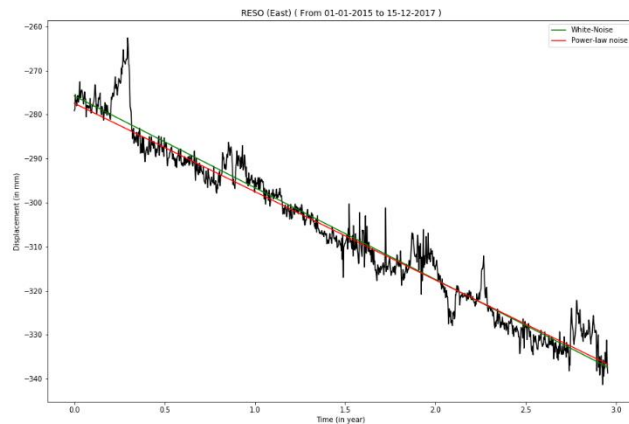
Figure 16

5.1.16 RESO

- **Site Name:** RESO
- **Location:** 74.6908201876 N, -118.6764300401 E
- **Start Date:** 01-01-2015
- **End Date:** 15-12-2017



Northern Component

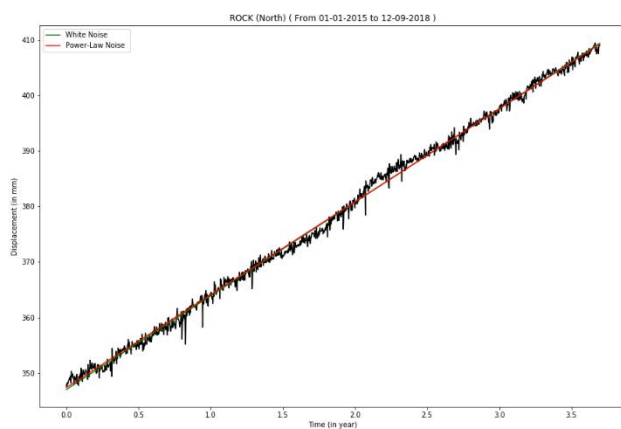


Eastern Component

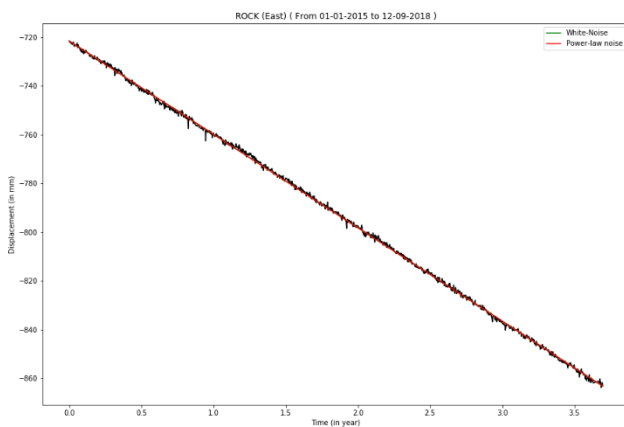
Figure 17

5.1.17 ROCK

- **Site Name:** ROCK
- **Location:** 34.2356740341 N, -118.6764300401 E
- **Start Date:** 01-01-2015
- **End Date:** 12-09-2018



Northern Component

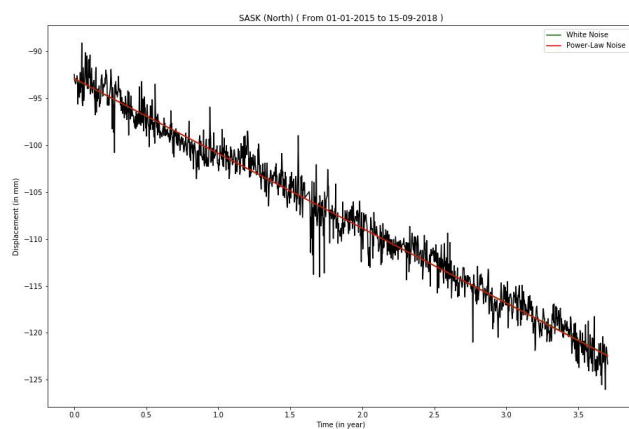


Eastern Component

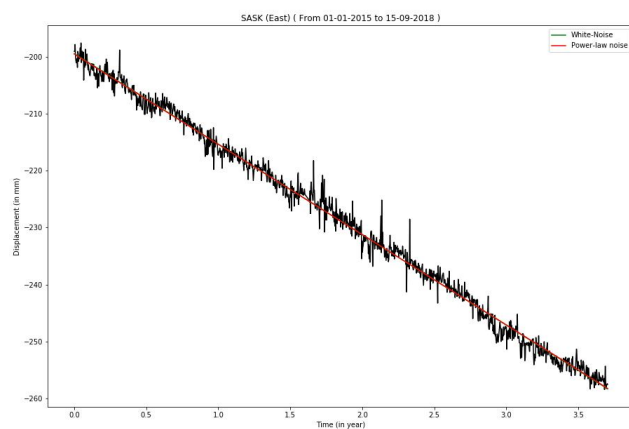
Figure 18

5.1.18 SASK

- **Site Name:** SASK
- **Location:** 52.1962546588 N, -106.3983555189 E
- **Start Date:** 01-01-2015
- **End Date:** 15-09-2018



Northern Component

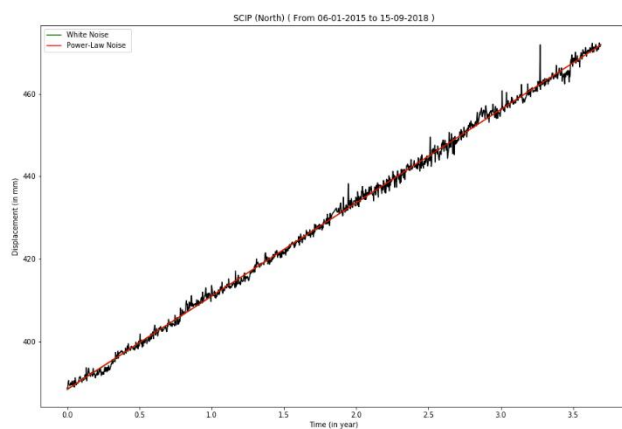


Eastern Component

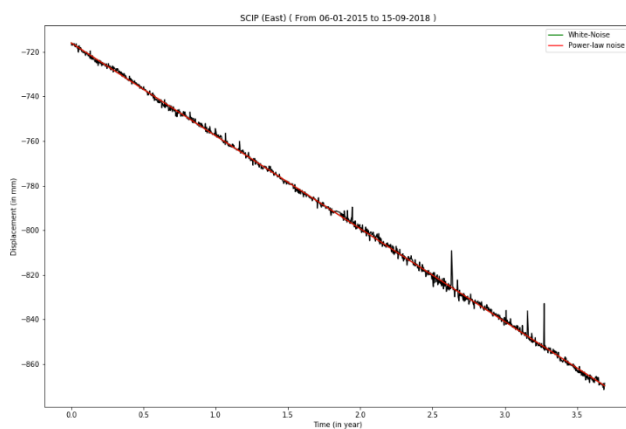
Figure 19

5.1.19 SCIP

- **Site Name:** SCIP
- **Location:** 32.9144276458 N, -118.4879389522 E
- **Start Date:** 06-01-2015
- **End Date:** 15-09-2018



Northern Component

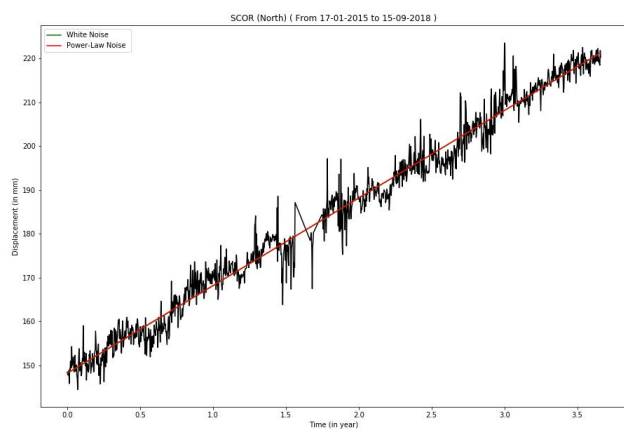


Eastern Component

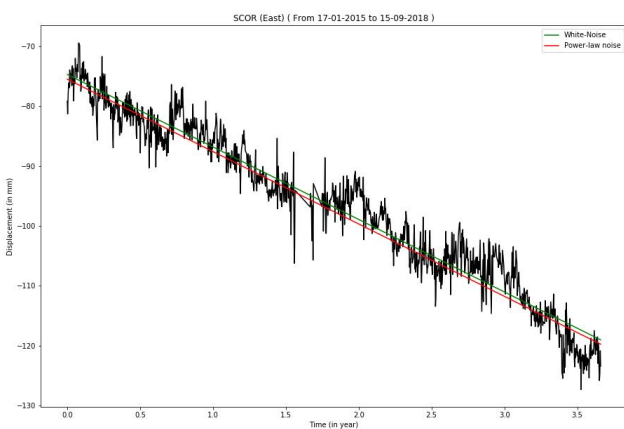
Figure 20

5.1.20 SCOR

- **Site Name:** SCOR
- **Location:** 70.4853345417 N, -21.9503379005 E
- **Start Date:** 17-01-2015
- **End Date:** 15-09-2018



Northern Component

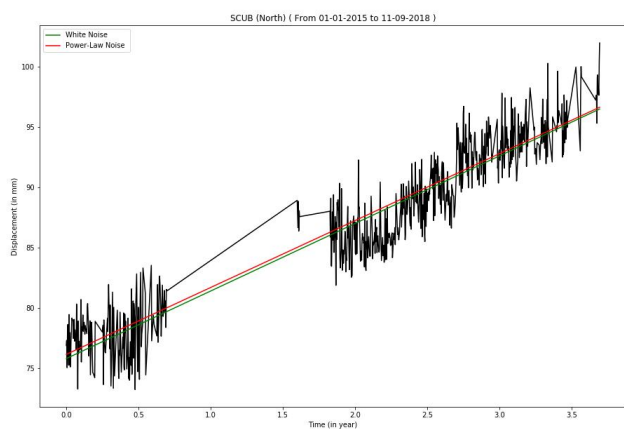


Eastern Component

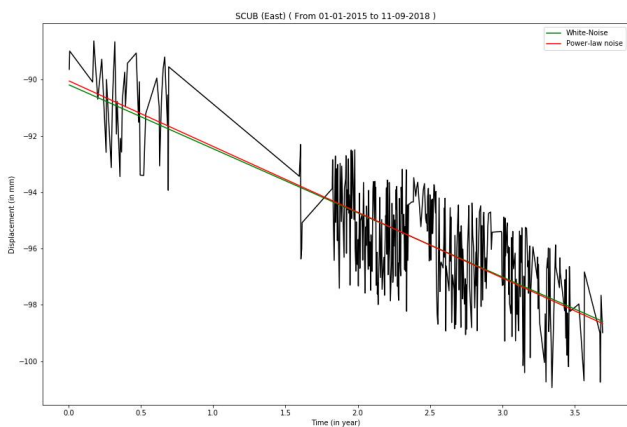
Figure 21

5.1.21 SCUB

- **Site Name:** SCUB
- **Location:** 20.0120635401 N, -75.7623166233 E
- **Start Date:** 01-01-2015
- **End Date:** 11-09-2018



Northern Component

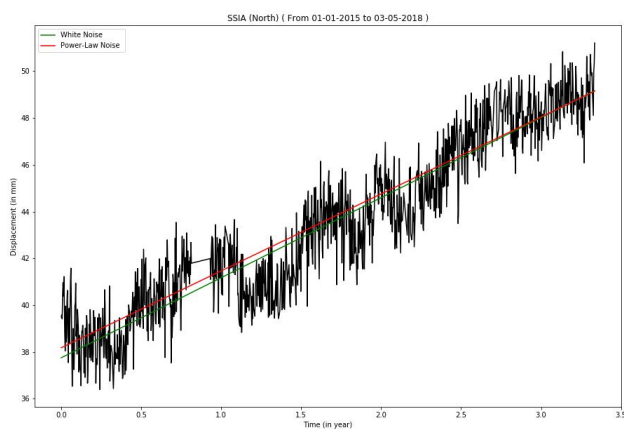


Eastern Component

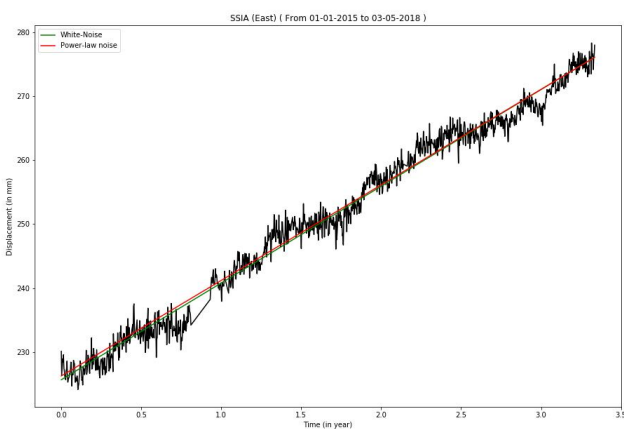
Figure 22

5.1.22 SSIA

- **Site Name:** SSIA
- **Location:** 13.6970852355 N, -89.1165949486 E
- **Start Date:** 01-01-2015
- **End Date:** 03-05-2018



Northern Component

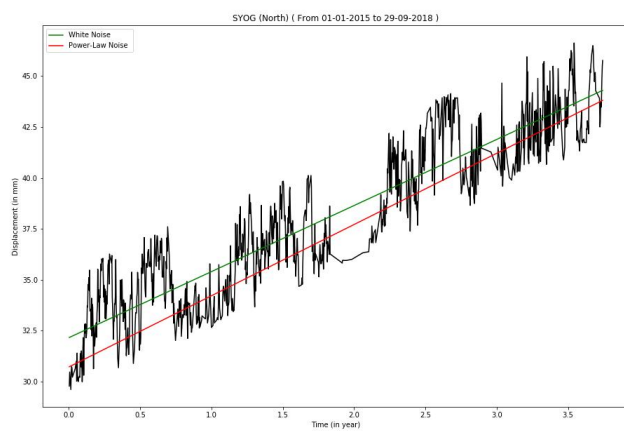


Eastern Component

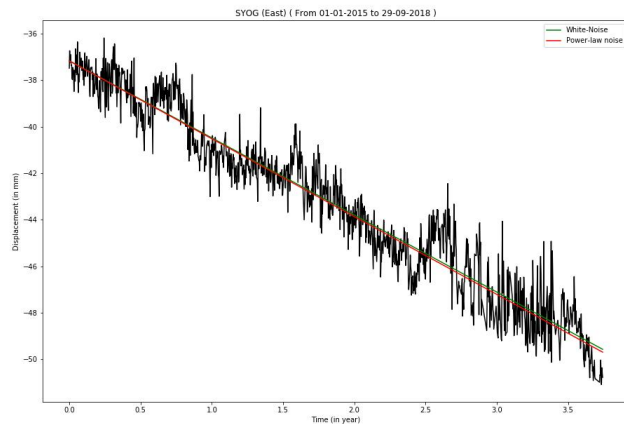
Figure 23

5.1.23 SYOG

- **Site Name:** SYOG
- **Location:** -69.0069570924 N, 39.5837429814 E
- **Start Date:** 01-01-2015
- **End Date:** 29-09-2018



Northern Component

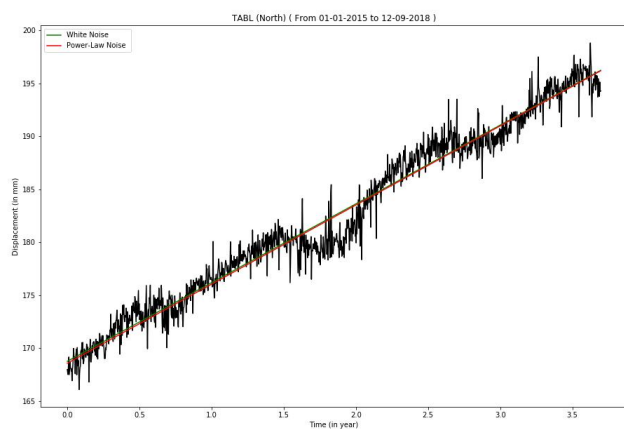


Eastern Component

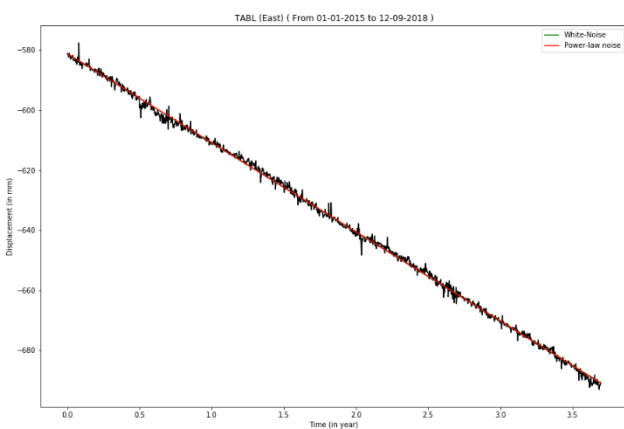
Figure 24

5.1.24 TABL

- **Site Name:** TABL
- **Location:** 34.3818486437 N, -117.6782815256 E
- **Start Date:** 01-01-2015
- **End Date:** 12-09-2018



Northern Component

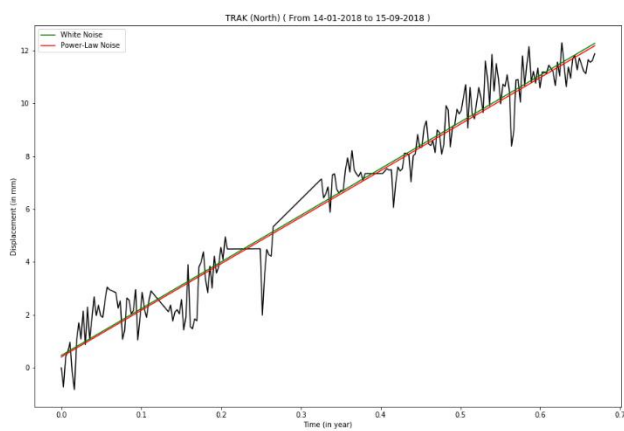


Eastern Component

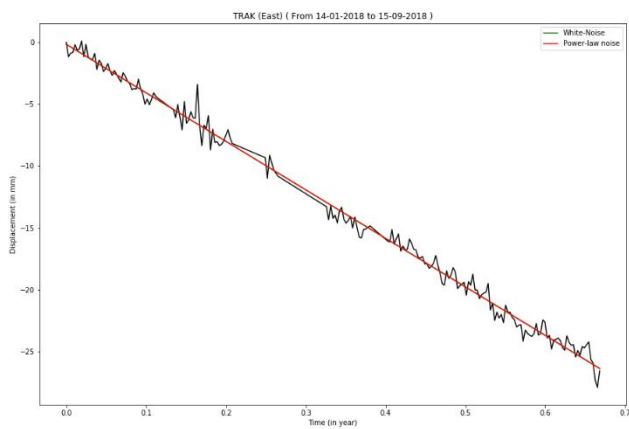
Figure 25

5.1.25 TRAK

- **Site Name:** TRAK
- **Location:** 33.6179380068 N, -117.803437812 E
- **Start Date:** 04-01-2018
- **End Date:** 15-09-2018



Northern Component

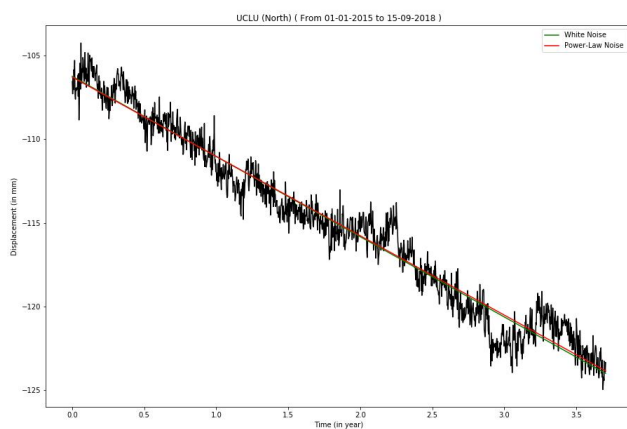


Eastern Component

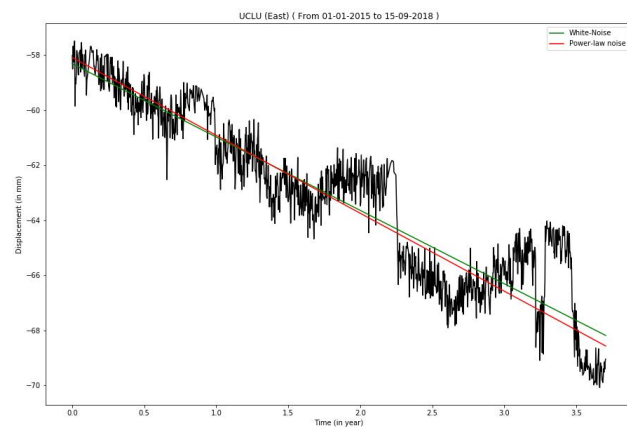
Figure 26

5.1.26 UCLU

- **Site Name:** UCLU
- **Location:** 48.9256375806 N, -125.5416410653 E
- **Start Date:** 01-01-2015
- **End Date:** 15-09-2018



Northern Component

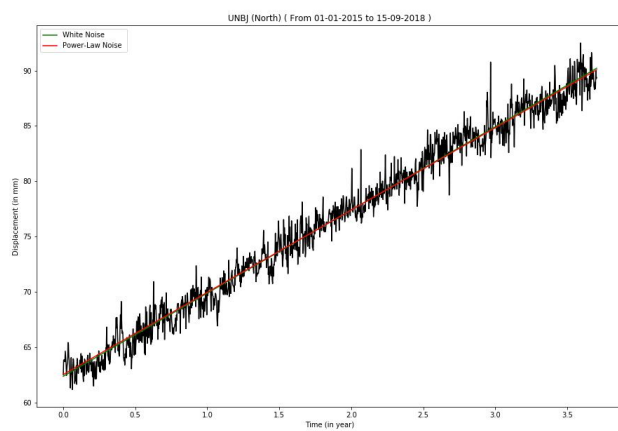


Eastern Component

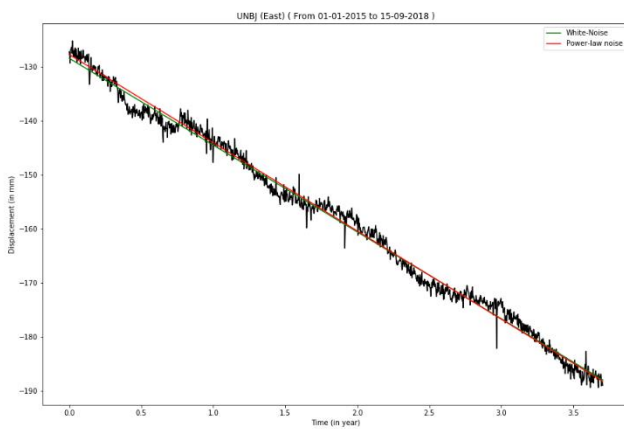
Figure 27

5.1.27 UNBJ

- **Site Name:** UNBJ
- **Location:** 45.9502093181 N, -66.6417052075 E
- **Start Date:** 01-01-2015
- **End Date:** 15-09-2018



Northern Component



Eastern Component

Figure 28

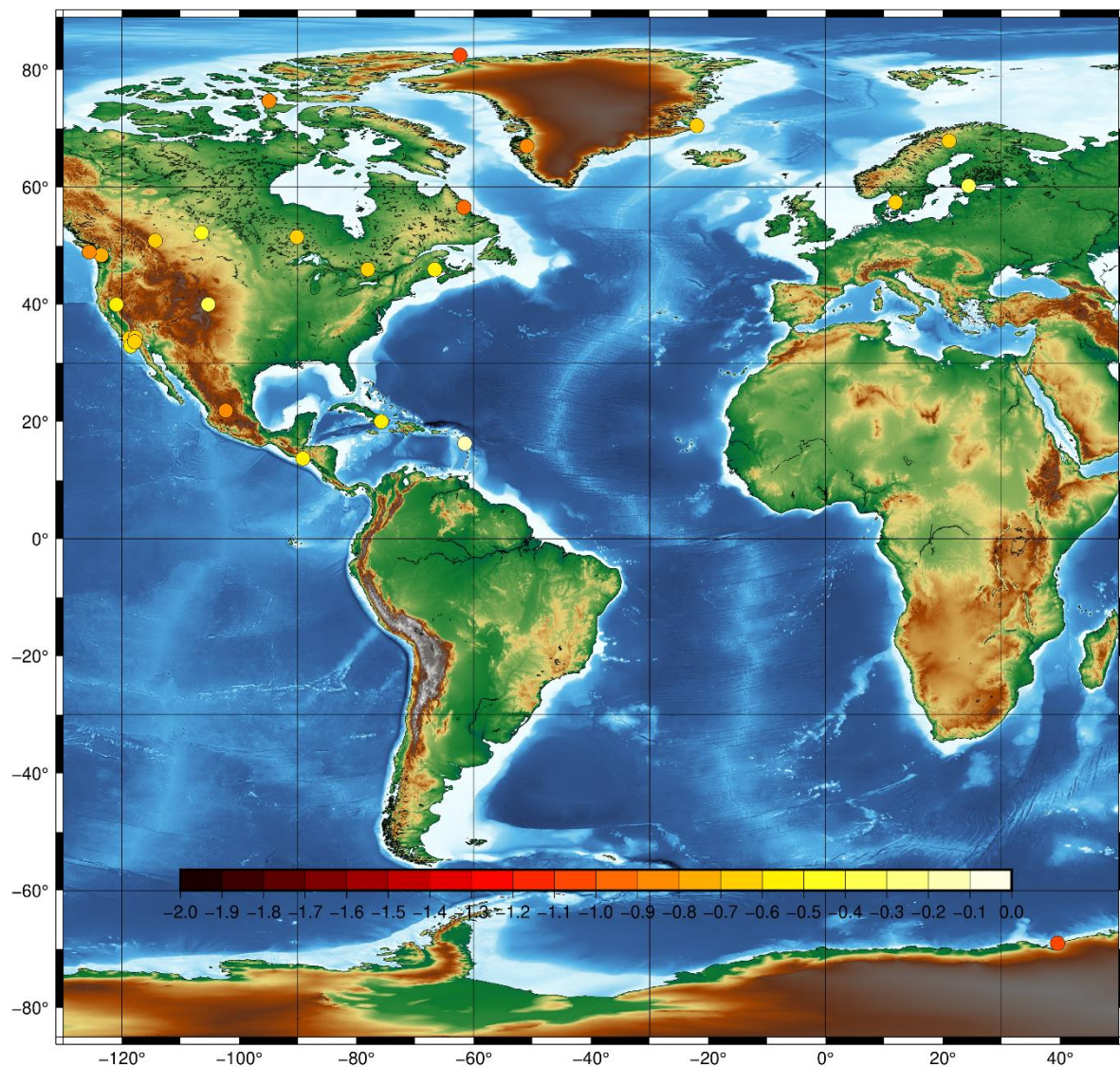
Site Name	White Noise			
	North		East	
	V (mm/year)	+/-	V (mm/year)	+/-
ABMF	14.693	0.044	10.506	0.043
ALBH	-7.623	0.026	-8.007	0.039
ALGO	2.229	0.024	-16.152	0.05
ALRT	8.206	0.051	-20.396	0.05
INEG	3.439	0.04	-8.403	0.07
JPLM	10.664	0.235	-35.635	0.278
KELY	12.115	0.044	-17.426	0.042
KIRO	-5.342	0.033	10.241	0.035
METS	14.424	0.747	21.629	0.888
NAIN	9.99	0.047	-15.959	0.052
NIST	-8.278	0.309	-18.755	0.392
ONSA	-6.408	0.035	15.1	0.034
PICL	-1.278	0.017	-1.09	0.02
PRDS	-0.971	0.013	1.913	0.016
QUIN	6.942	0.022	-7.788	0.03
RESO	-4.631	0.077	-20.847	0.133
ROCK	16.876	0.025	-38.29	0.02
SASK	-7.943	0.034	-15.902	0.035
SCIP	22.606	0.026	-41.663	0.033
SCOR	19.989	0.08	-12.24	0.078
SCUB	5.628	0.073	-1.726	0.092
SSIA	3.744	0.04	15.122	0.056
SYOG	2.696	0.048	-3.371	0.025
TABL	7.427	0.035	-29.649	0.028
TRAK	17.654	0.269	-39.221	0.229
UCLU	-4.786	0.025	-2.664	0.03

Table 2: Estimated velocity using white noise method along with the uncertainties.

Site Name	Power Law Noise							
	North				East			
	V (mm/year)	+/-	Spectral Index (- κ)	Noise Amplitude(σ_{pl})	V (mm/year)	+/-	Spectral Index (- κ)	Noise Amplitude(σ_{pl})
ABMF	14.693	0.063	-0.13	2.814	10.424	0.124	-0.411	2.573
ALBH	-7.529	0.152	-0.789	0.725	-8.022	0.272	-0.972	0.786
ALGO	2.329	0.111	-0.645	0.738	-15.929	0.78	-1.145	1.347
ALRT	8.109	0.551	-1.068	1.178	-20.965	0.417	-0.984	1.16
INEG	3.252	0.23	-0.898	0.739	-8.679	0.378	-0.99	1.012
JPLM	10.778	0.577	-0.614	0.566	-35.834	0.615	-0.506	0.735
KELY	12.047	0.306	-0.801	1.293	-17.073	0.411	-0.982	1.059
KIRO	-5.407	0.182	-0.696	1.657	9.909	0.332	-0.934	1.556
METS	14.648	1.22	-0.328	1.84	21.71	2.094	-0.582	2.162
NAIN	9.651	0.418	-0.936	1.347	-15.771	0.664	-1.083	1.411
NIST	-8.325	0.557	-0.381	0.783	-18.723	0.686	-0.334	1.09
ONSA	-6.543	0.209	-0.688	1.971	15.008	0.255	-0.811	1.701
PICL	-1.256	0.077	-0.628	0.78	-1.01	0.119	-0.748	0.89
PRDS	-0.978	0.062	-0.619	0.673	1.898	0.082	-0.734	0.644
QUIN	6.918	0.095	-0.56	1.314	-7.819	0.185	-0.82	1.228
RESO	-4.446	0.483	-0.87	1.425	-20.065	1.77	-1.22	1.923
ROCK	16.735	0.114	-0.653	0.775	-38.276	0.079	-0.561	0.683
SASK	-7.979	0.112	-0.461	1.275	-15.851	0.137	-0.549	1.236
SCIP	22.565	0.111	-0.576	0.929	-41.66	0.073	-0.297	1.276
SCOR	19.965	0.414	-0.683	2.6	-12.189	0.441	-0.769	2.192
SCUB	5.577	0.212	-0.518	1.869	-1.866	0.184	-0.41	1.358
SSIA	3.673	0.144	-0.557	1.072	14.934	0.303	-0.774	1.346
SYOG	3.02	0.489	-1.081	1.022	-3.392	0.145	-0.745	0.769
TABL	7.463	0.173	-0.697	1.057	-29.684	0.123	-0.594	0.984
TRAK	17.599	0.797	-0.693	0.692	-39.258	0.431	-0.377	0.645
UCLU	-4.733	0.164	-0.848	0.67	-2.828	0.277	-1.081	0.579
UNBJ	7.515	0.028	-16.059	0.038	7.434	0.12	-0.57	1.029

Table 3: Estimated velocity using power-law noise method along with the uncertainties.

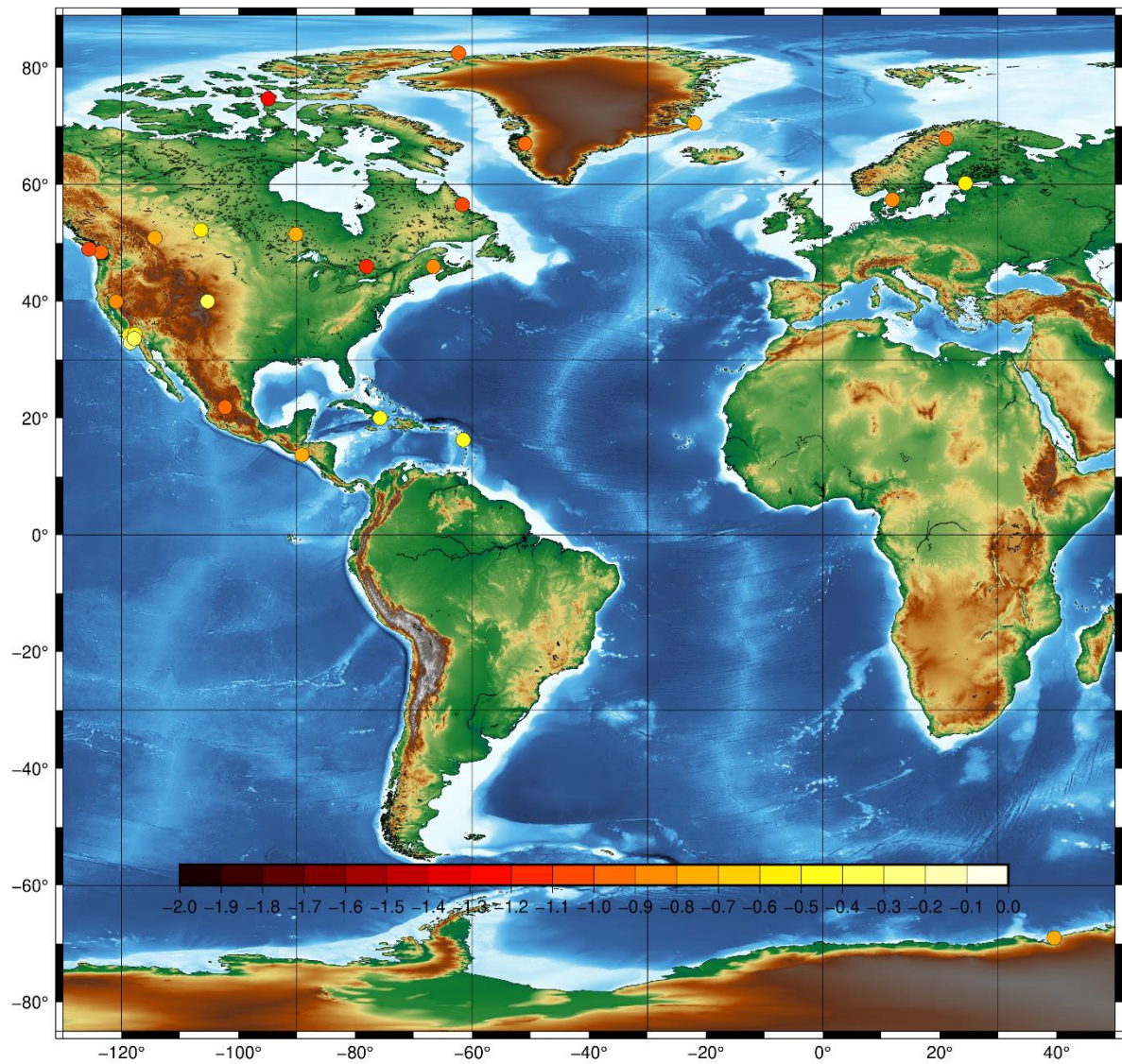
Spectral Index for North Component



GMD 2020 Jun 09 03:30:54

Figure 29 Spectral Index for the North-Component of the Time-Series of the different GPS-Sites

Spectral Index for East Component



GMD 2020 Jun 09 03:31:49

Figure 30 Spectral Index for the East-Component of the Time-Series of the different GPS-Sites

5.2 Markov Chain Monte Carlo (MCMC)

Site Name	Markov Chain Monte Carlo(MCMC)			
	North		East	
	V (mm/year)	+/-	V (mm/year)	+/-
ABMF	14.672	0	10.521	0.045
ALBH	-7.624	0.026	-8.011	0.039
ALGO	2.165	0.024	-16.165	0.05
ALRT	8.003	0.051	-20.273	0.048
INEG	3.437	0.041	-8.417	0.071
JPLM	10.615	0.229	-35.608	0.287
KELY	12.124	0.046	-17.435	0.044
KIRO	-5.08	0.037	10.246	0.036
METS	14.344	0.779	21.492	0.911
NAIN	10.145	0.046	-15.961	0.051
NIST	-8.027	0.298	-19.361	0.357
ONSA	-6.42	0.036	15.109	0.034
PICL	-1.278	0.018	-1.09	0.022
PRDS	-1.052	0.014	1.912	0.016
QUIN	6.944	0.022	-7.744	0.03
RESO	-4.637	0.078	-20.916	0.136
ROCK	16.879	0.026	-38.368	0.143
SASK	-7.944	0.035	-15.908	0.035
SCIP	22.612	0.027	-41.679	0.035
SCOR	20.005	0.082	-12.115	0.081
SCUB	5.605	0.076	-2.297	0.09
SSIA	3.423	0.04	15.136	0.056
SYOG	3.247	0.046	-3.314	0.025
TABL	7.432	0.036	-29.657	0.029
TRAK	17.634	0.279	-39.199	0.233
UCLU	-4.788	0.026	-2.596	0.031
UNBJ	7.516	0.029	-16.063	0.039

Table 4: Estimated velocity using Markov Chain Monte Carlo (MCMC) method.

Interpretation and Results

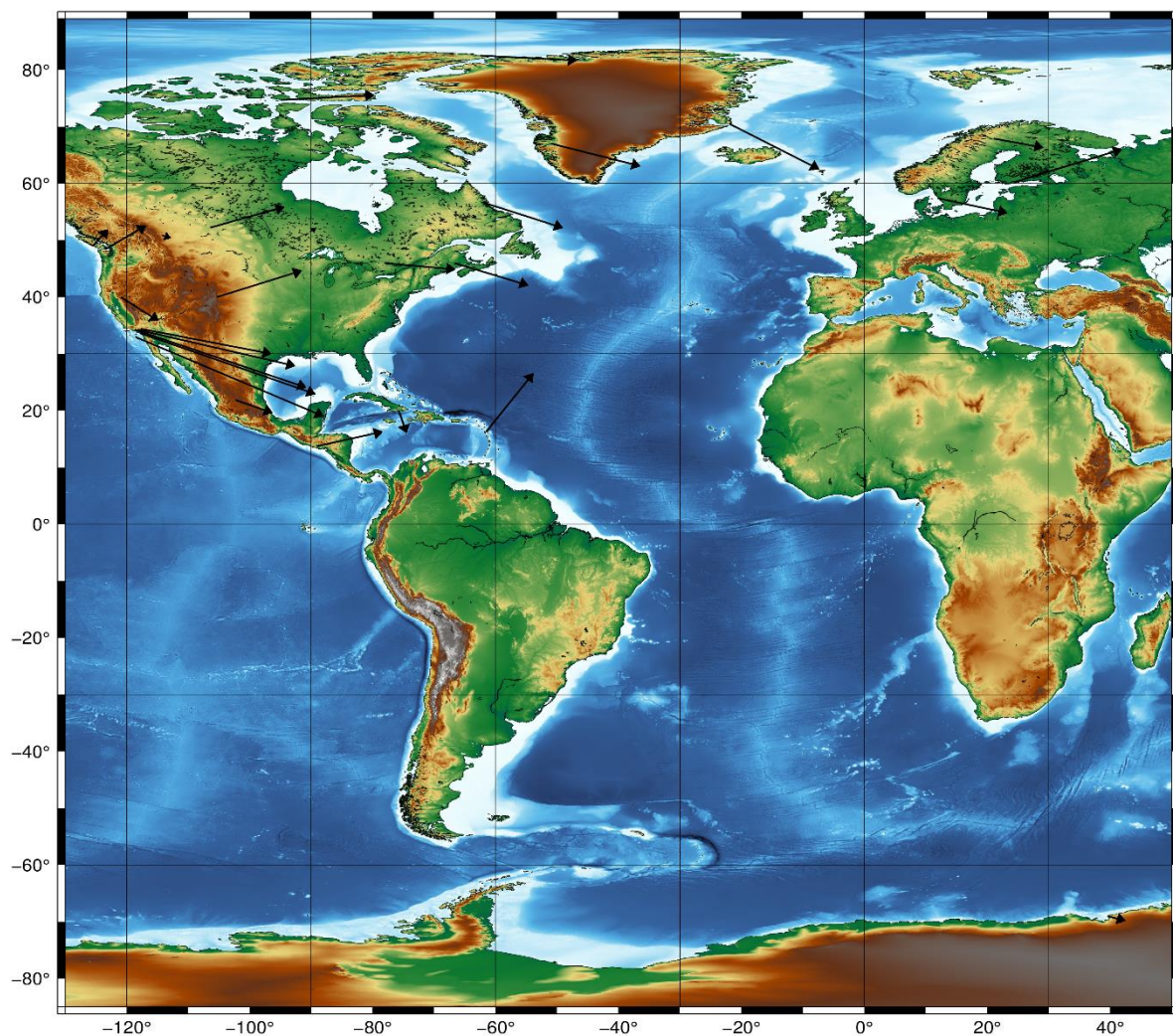
White noise method is not used ideally, as there is temporal correlation between the noises in our data. Power-Law noise is one of the most widely modelling method used in geodetic time series analysis. Therefore, we are only comparing Power-Law Noise and MCMC Methods only.

On comparison of Northern velocity component, the maximum difference was found to be about 0.494 mm/year from site **NAIN**, minimum difference was about 0.021 mm/year from site **ABMF**. The average difference was about 0.134 that is quiet small.

While comparison of Eastern velocity component, the maximum difference was found to be about 0.851 mm/year from site **RESO**, minimum difference was about 0.011 mm/year from site **ALBH**. The average difference was about 0.219 that is also quiet small.

Therefore, we can estimate our velocity using both the methods efficiently. We have plotted the velocities obtained from our analysis below and compared the estimated velocities from the different methods in Table 5 and Table 6.

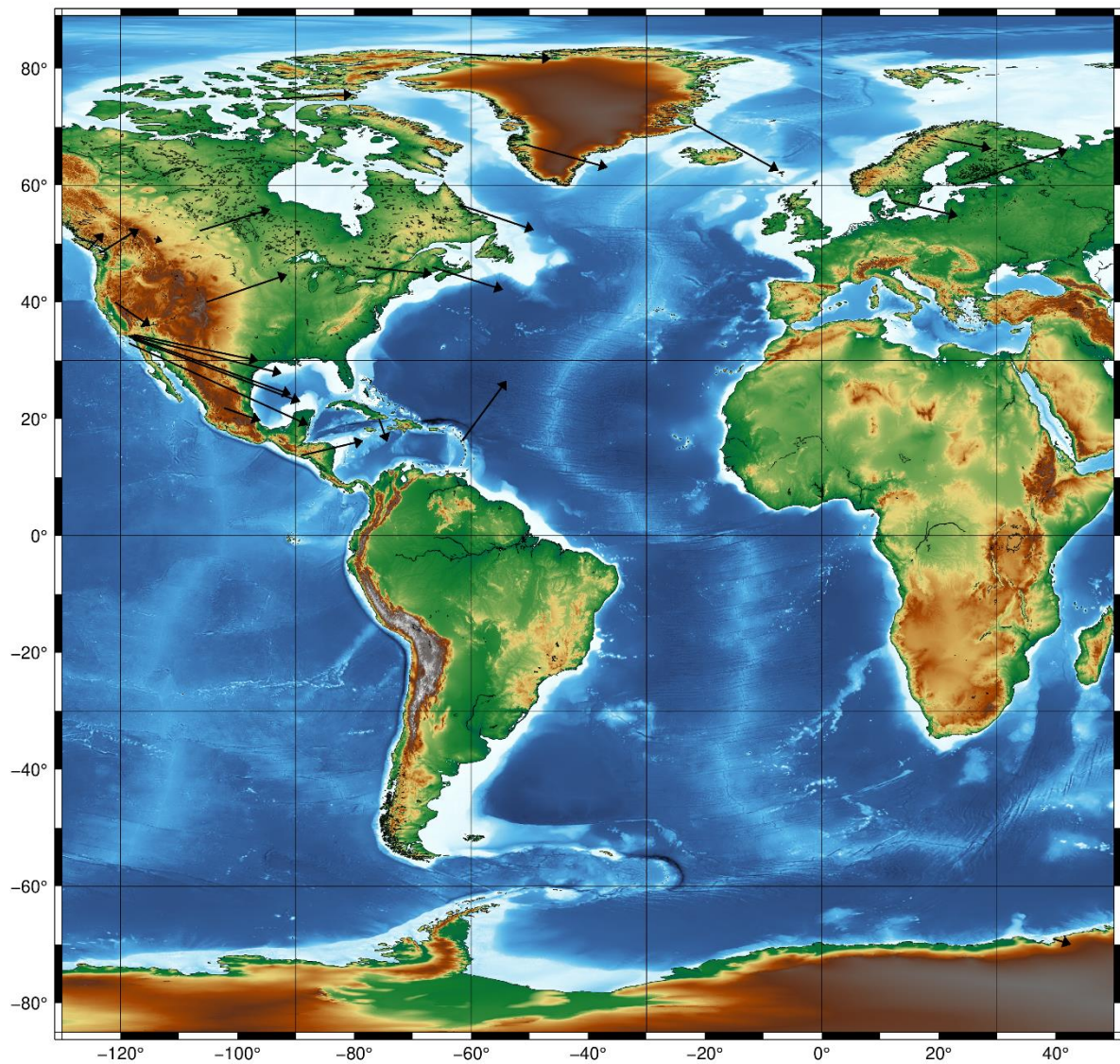
White Noise Velocity



GM 2020 Jun 09 02:15:43

Figure 31 Velocity estimated from the White Noise Method.

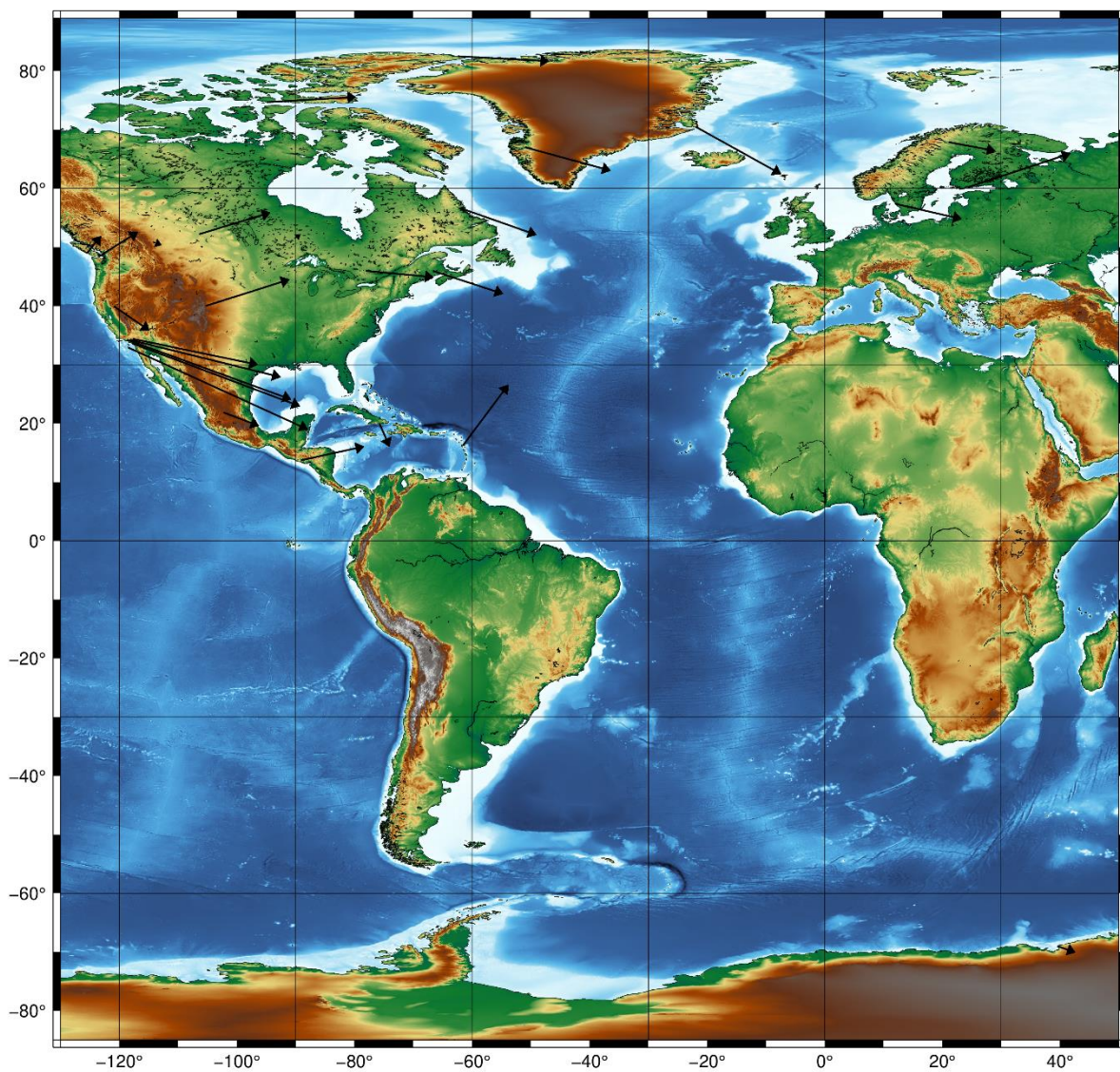
Power Noise Velocity



GMD 2020 Jun 09 02:16:14

Figure 32 Velocity estimated from the Power Law Noise Method.

Velocity Estimates from Markov Chain Monte Carlo (MCMC)



GMD 2020 Jun 09 02:23:24

Figure 33 Velocity estimated from the MCMC Method.

Site Name	North					
	V (mm/year)			Difference		
	White Noise	Power-Law Noise	MCMC	WN & PLN	WN & MCMC	PLN & MCMC
ABMF	14.693	14.693	14.672	0	0.021	0.021
ALBH	-7.623	-7.529	-7.624	0.094	0.001	0.095
ALGO	2.229	2.329	2.165	0.1	0.064	0.164
ALRT	8.206	8.109	8.003	0.097	0.203	0.106
INEG	3.439	3.252	3.437	0.187	0.002	0.185
JPLM	10.664	10.778	10.615	0.114	0.049	0.163
KELY	12.115	12.047	12.124	0.068	0.009	0.077
KIRO	-5.342	-5.407	-5.08	0.065	0.262	0.327
METS	14.424	14.648	14.344	0.224	0.08	0.304
NAIN	9.99	9.651	10.145	0.339	0.155	0.494
NIST	-8.278	-8.325	-8.027	0.047	0.251	0.298
ONSA	-6.408	-6.543	-6.42	0.135	0.012	0.123
PICL	-1.278	-1.256	-1.278	0.022	0	0.022
PRDS	-0.971	-0.978	-1.052	0.007	0.081	0.074
QUIN	6.942	6.918	6.944	0.024	0.002	0.026
RESO	-4.631	-4.446	-4.637	0.185	0.006	0.191
ROCK	16.876	16.735	16.879	0.141	0.003	0.144
SASK	-7.943	-7.979	-7.944	0.036	0.001	0.035
SCIP	22.606	22.565	22.612	0.041	0.006	0.047
SCOR	19.989	19.965	20.005	0.024	0.016	0.04
SCUB	5.628	5.577	5.605	0.051	0.023	0.028
SSIA	3.744	3.673	3.423	0.071	0.321	0.25
SYOG	2.696	3.02	3.247	0.324	0.551	0.227
TABL	7.427	7.463	7.432	0.036	0.005	0.031
TRAK	17.654	17.599	17.634	0.055	0.02	0.035
UCLU	-4.786	-4.733	-4.788	0.053	0.002	0.055
UNBJ	7.515	7.434	7.516	0.081	0.001	0.082

Table 5: Comparison of the North-Component of the velocities estimated using different methods.

Site Name	East					
	V (mm/year)			Difference		
	White Noise	Power-Law Noise	MCMC	WN & PLN	WN & MCMC	PLN & MCMC
ABMF	10.506	10.424	10.521	0.082	0.015	0.097
ALBH	-8.007	-8.022	-8.011	0.015	0.004	0.011
ALGO	-16.152	-15.929	-16.165	0.223	0.013	0.236
ALRT	-20.396	-20.965	-20.273	0.569	0.123	0.692
INEG	-8.403	-8.679	-8.417	0.276	0.014	0.262
JPLM	-35.635	-35.834	-35.608	0.199	0.027	0.226
KELY	-17.426	-17.073	-17.435	0.353	0.009	0.362
KIRO	10.241	9.909	10.246	0.332	0.005	0.337
METS	21.629	21.71	21.492	0.081	0.137	0.218
NAIN	-15.959	-15.771	-15.961	0.188	0.002	0.19
NIST	-18.755	-18.723	-19.361	0.032	0.606	0.638
ONSA	15.1	15.008	15.109	0.092	0.009	0.101
PICL	-1.09	-1.01	-1.09	0.08	0	0.08
PRDS	1.913	1.898	1.912	0.015	0.001	0.014
QUIN	-7.788	-7.819	-7.744	0.031	0.044	0.075
RESO	-20.847	-20.065	-20.916	0.782	0.069	0.851
ROCK	-38.29	-38.276	-38.368	0.014	0.078	0.092
SASK	-15.902	-15.851	-15.908	0.051	0.006	0.057
SCIP	-41.663	-41.66	-41.679	0.003	0.016	0.019
SCOR	-12.24	-12.189	-12.115	0.051	0.125	0.074
SCUB	-1.726	-1.866	-2.297	0.14	0.571	0.431
SSIA	15.122	14.934	15.136	0.188	0.014	0.202
SYOG	-3.371	-3.392	-3.314	0.021	0.057	0.078
TABL	-29.649	-29.684	-29.657	0.035	0.008	0.027
TRAK	-39.221	-39.258	-39.199	0.037	0.022	0.059
UCLU	-2.664	-2.828	-2.596	0.164	0.068	0.232
UNBJ	-16.059	-16.32	-16.063	0.261	0.004	0.257

Table 6: Comparison of the East-Component of the velocities estimated using different methods.

References

Granger C (1980) Long memory relationships and the aggregation of dynamic models. Journal of Econometrics 14(2):227 – 238, [https://doi.org/10.1016/0304-4076\(80\)90092-5](https://doi.org/10.1016/0304-4076(80)90092-5)

Granger CWJ, Joyeux R (1980) An Introduction to Long-Memory Time Series Models and Fractional Differencing. Journal of Time Series Analysis 1(1):15–29, <https://doi.org/10.1111/j.1467-9892.1980.tb00297.x>

Hosking JRM (1981) Fractional differencing. Biometrika 68:165–176

Kasdin NJ (1995) Discrete simulation of colored noise and stochastic processes and $1/f^\alpha$ power-law noise generation. Proc IEEE 83(5):802–827

Geodetic Time Series Analysis in Earth Sciences by Jean-Philippe Montillet and Machiel S. Bos.
(<https://www.springer.com/gp/book/9783030217174>).